Results in Physics 18 (2020) 103258

Contents lists available at ScienceDirect

Results in Physics

journal homepage: www.elsevier.com/locate/rinp

Thermally induced evolution of the structure and optical properties of silicon nanowires

Gauhar Mussabek[a,b,g,*], Vladimir Lysenko[b,c], Dana Yermukhamed[a], Vladimir Sivakov[d], Victor Yu. Timoshenko[b,e,f]

[a] Al-Farabi Kazakh National University, Faculty of Physics and Technology, 71, Al-Farabi Ave., 050040 Almaty, Kazakhstan
[b] National Research Nuclear University MEPhI (Moscow Engineering Physics Institute), PhysBio Institute, Kashirskoe sh. 31, 115409 Moscow, Russia
[c] Light Matter Institute, UMR-5306, Claude Bernard University of Lyon, 2 rue Victor Grignard, 69622 Villeurbanne, France
[d] Leibniz Institute of Photonic Technology, Albert-Einstein-Str. 9, 07745 Jena, Germany
[e] Lomonosov Moscow State University, Leninskie Gory 1, 119991 Moscow, Russia
[f] Lebedev Physical Institute of the Russian Academy of Sciences, 53 Leninskiy Pr., 119991 Moscow Russia
[g] Institute of Information and Computational Technologies, 125, Pushkin Str., 050000 Almaty, Kazakhstan

ARTICLE INFO

Keywords:
Silicon
Nanowires
Metal assisted etching
Thermal annealing
Ostwald ripening

ABSTRACT

In the present paper, we report on the investigation of thermal annealing (TA) effect on structural and optical properties of crystalline silicon nanowires produced by metal-assisted chemical etching approach. In particular, the impact of TA on nanowire length, relative volume and size distribution of voids is described in terms of Lifshitz-Slyozov-Wagner theory considering the TA induced Oswald ripening in the SiNW arrays. It was also found that TA leads to a decrease of the SiNWs total reflection in the wide UV–VIS-IR spectral range. The reported effects can be used for tuning of crystalline SiNWs arrays in view of their further applications in photonics related fields.

Introduction

Silicon nanowires (SiNWs) have attracted considerable interest due to their potential applications in different fields including micro- and nanoelectronics [1,2], photovoltaics [3–5], thermoelectrical devices [6,7] and nanomedicine [8–10]. Several methods based on “bottom-up” and “top-down” technologies [11,12] have been successfully developed to prepare SiNWs with desired lengths and cross-sectional sizes. Metal-assisted chemical etching (MACE) [13,14] is a “top-down” approach which has become the most used one in the last decade due to its gaining better fabrication and relatively low cost. MACE technology is based on the selective chemical dissolution of crystalline silicon (c-Si) in hydrofluoric acid (HF) solutions that is assisted by the noble metal nanoparticles, e.g. silver, gold, copper etc., as a catalyst. The morphology of resulting SiNWs arrays can be controlled *via* altering the MACE conditions.

One of the widely discussed characteristics, related to the SiNWs properties is their unique optical properties in comparison to the bulk c-Si [15]. Crystalline SiNWs array demonstrates strong broadband optical absorption in the full visible spectral range due an effect to the “light trapping” leading to a strong suppression of the optical reflection in the spectral region of the band gap absorption in c-Si [16]. It is well-known, from previously published works, that MACE-prepared SiNW arrays by their optical properties can be referred to so-called “black” and “white” SiNWs [16,17]. Notably, the “black” SiNW arrays act as an excellent absorber in the visible and UV spectral range [18,19], while the “white” samples exhibit a high level of the diffuse optical reflection in the near IR spectral region [17]. These optical properties of SiNWs are proposed to be used in a stealth sheet technology [20].

Thermal annealing (TA) is the well-known treatment, which is widely used in different technological processing of c-Si. However, there is currently a lack of detailed studies of TA induced changes in SiNWs and some basic problems such as restructuring and sintering mechanisms remain unclear. Despite various efforts to understand the nature of “black” and “white” silicon surfaces prepared by MACE [21,22]. Exploring possible mechanisms of TA-induced modifications of the structural and optical properties of SiNWs will help to explain the fundamental aspects of various phenomena in 1D nanostructures and it can be useful for applications of SiNWs in photovoltaics [23], sensors [24] and thermoelectric power converters [25].

In the present paper, an extended analysis of the structural properties of crystalline SiNW arrays, which are modified by short-term

* Corresponding author at: Al-Farabi Kazakh National University, Faculty of Physics and Technology, 71, Al-Farabi Ave., 050040 Almaty, Kazakhstan.
E-mail address: gauhar.musabek@kaznu.kz (G. Mussabek).

https://doi.org/10.1016/j.rinp.2020.103258
Received 13 June 2020; Received in revised form 19 July 2020; Accepted 20 July 2020
Available online 29 July 2020

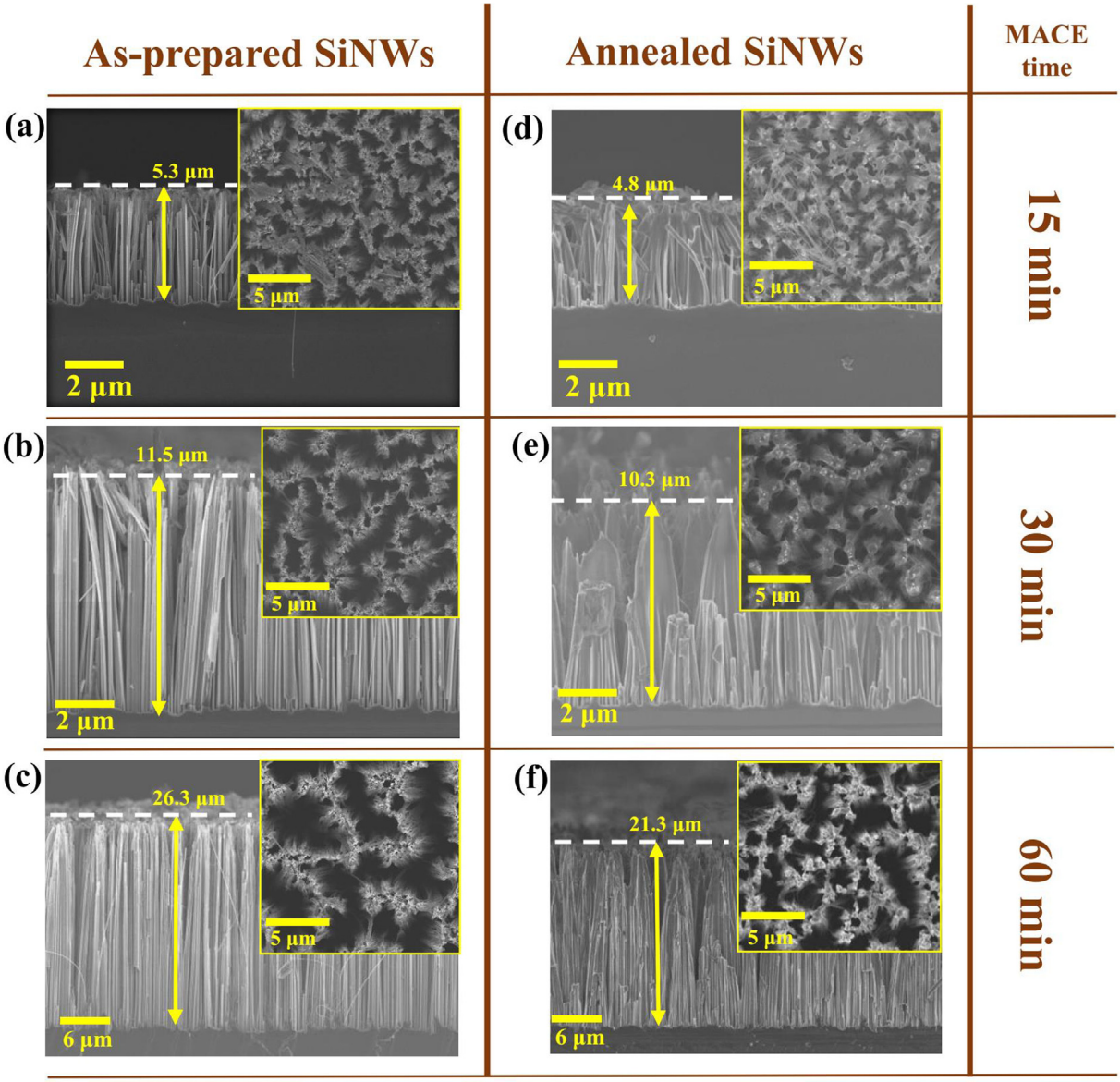

Fig. 1. Cross sectional and corresponding planar (insets) SEM images of SiNWs obtained for 15, 30 and 60 min of MACE process before (a), (b), (c) and after (d), (e), (f) thermal annealing, respectively. Dashed lines indicate surface level.

thermal annealing, has been performed. In particular, the role of the initial length of SiNWs on the thermally induced reorganization of the whole nanowires arrays is described in detail. The obtained results are explained in terms of the Oswald ripening phenomena and Lifshitz-Slyozov-Wagner (LSW) theory [26–28].

Materials and methods

SiNWs were fabricated by wet-chemical etching of lowly boron doped single crystalline Si (c-Si) wafers with a (100) crystalline orientation and a specific resistance of 1–10 Ω cm. Initially, the c-Si substrates were rinsed in 2% HF solution for 5 min to remove native oxide. Silver (Ag) nanoparticles were used as catalysts in the MACE process. The first step of MACE was related to the deposition of Ag nanoparticles on the wafer surfaces by immersing them in a mixture of aqueous solutions of 0.02 M $AgNO_3$ and 5 M HF (1:1, v/v) for 30 s. Further etching of the c-Si wafers with deposited Ag nanoparticles was performed in the following solution [HF (5 M): H_2O_2 (30%)] = 10:1. To obtain SiNWs layers of different thicknesses, the duration of the MACE process was varied from 15 to 60 min. After etching, the Ag nanoparticles were removed with nitric acid (HNO_3, 65%), after which the samples were washed with deionized water and air-dried. All steps of the etching process were performed at room temperature conditions. The thermal annealing (TA) of SiNWs was performed at 900 °C temperature for 10 min in air.

The structural properties and morphology of as-prepared and TA-treated SiNWs were investigated by using a Carl Zeiss Ultra 55 field emission scanning electron microscope (FE-SEM). To obtain the pore size distribution, a quantitative analysis of the achieved SEM images was performed using the ImageJ software. Recently it was shown that determination of porosity of Si nanostructures by image processing of top-view SEM micrographs corresponded well to the results of porosity measurements by gravimetric and nitrogen absorption methods [29]. Furthermore, the porosity of SiNW arrays estimated from the value of effective refractive index was shown to agree with the SEM image analysis [30].

The structural properties of SiNWs were studied by using means of the Raman spectroscopy. The Raman spectra were recorded with a Solver Spectrum (NT-MDT) Raman spectrometer under laser excitation at a wavelength of 473 nm with intensity of 0.2 mW/cm^2. The

acquisition time of each Raman spectrum was 10 s and the diameter of the laser spot was about 2 μm. The measurements were carried out in air at room temperature.

Optical properties of as-prepared and TA treated samples were investigated by means of the total reflection spectra measurements in a UV–vis/NIR spectrometer (Jasco V-670) equipped with an ISN-923 60 mm integrating sphere accessory. The total reflection was measured in the spectral range from 300 to 2000 nm.

Results and discussion

SEM structural characterization

Thermally induced evolution of SiNWs length

Generally, the thermal treatment of porous materials or powders below the melting point is accompanied by structural and/or morphological changes [31]. In the case of porous silicon, for example, the corresponding thermally induced morphological changes can be observed at temperatures below 350 °C [31], which is significantly lower than the melting point of bulk Si (1412 °C) [32,33]. The driving force for this thermally induced reorganization is related to minimizing the surface energy of porous Si associated with its highly developed inner surface [31,34–36]. Similarly to the porous silicon, SiNWs array can also show a similar tendency of the structural rearrangement due to the annealing process below the melting point (sintering) of c-Si. It is known from the classical sintering theory developed for porous materials [28] that the thermal activation is necessary to stimulate atoms by forcing them to take more favourable energy positions, thereby reducing the surface-to-volume ratio.

Indeed, SiNWs array can be considered as a kind of porous Si in which vertically aligned voids between Si wires play the role of pores. Cross-sectional SEM images of as-prepared SiNWs and their corresponding planar views, obtained during 15, 30 and 60 min of MACE (see Fig. 1a, b and c respectively) and after TA at 900 °C during 10 min (see Fig. 1d, e and f respectively) are shown in Fig. 1. It is seen that as-prepared SiNW arrays possess a highly connected network of voids. As a result of the TA treatment, a significant reduction in the length of SiNWs appears. The average value of SiNWs layer thickness obtained by etching at 60 min is 26.3 μm, and after heat treatment, it decreases to 21.3 μm. Such a significant reduction in nanowires length (10–20%) was also observed for the samples obtained with a shorter etching times (see Fig. S1 in SM).

Thermally induced evolution of SiNWs morphology

Raman spectroscopy is well-known as an excellent non-destructive optical tool for studying the structural properties of nanomaterials, which have been used in present work to evaluate thermally induced structural changes in SiNWs arrays. Fig. 2 shows the normalized Raman spectra of as-prepared and TA treated SiNWs of different lengths. For comparison, the Raman spectrum of c-Si wafer is also given in Fig. 2 and it is centred at 520.5 cm^{-1} and characterized by the full width at half maximum (FWHM) of about 4 cm^{-1}. The spectral position and FWHM of Raman peaks of the short (5.3 μm) as-prepared and annealed SiNWs are slightly different from that of c-Si. The observed small shift of the Raman peak maximum to the lower frequency region and its broadening can be explained by the presence of nanosized Si structures with characteristic crystallites sizes ≥ 10 nm [37,38].

The Raman spectrum of as-prepared long SiNWs (26.3 μm) shows more downshifted Raman peak centred at 518 cm^{-1}, while Raman spectra of the annealed long SiNWs centred at 520 cm^{-1} that corresponds to the Raman peak of c-Si. Such more significant spectral redshift can evidence formation of nanostructured porous Si with characteristic crystallite sizes about 10 nm on the top of SiNW arrays [38,39]. The TA induced spectral shift of the Raman peak to higher energies indicates on explicit sintering of long nanowires with formation of bulk-like crystalline agglomerates as well as smoothing of rough

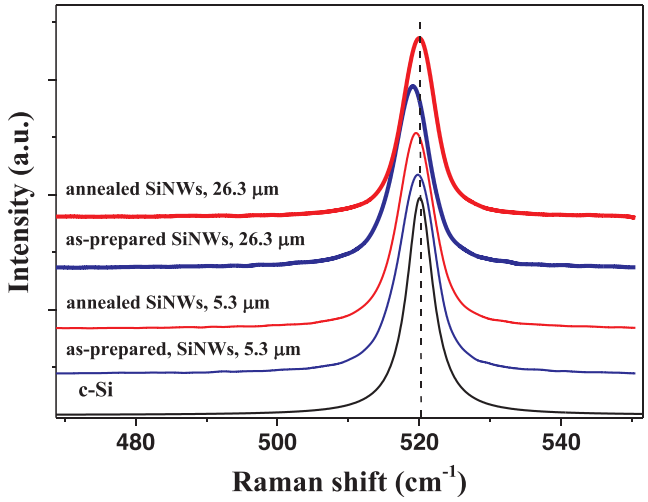

Fig. 2. Normalized Raman spectra of SiNWs with length of 5.3 μm (thin lines) and 26.3 μm (bold lines) before (blue lines) and after TA (red lines) as well for the corresponding c-Si substrate (black line).

porous SiNW sidewall structure in which quantum confinement effects may occur [40]. It is notable to mention that te Raman spectra of SiNWs arrays before and after TA exclude the presence of the amorphous phase (a-Si), which is usually manifested by a band at 480 cm^{-1} [34–37].

An analysis of the chemical composition of SiNWs performed by energy dispersive X-ray analysis (EDX) during the SEM studies showed that the TA treatment didn't result in any noticeable changes in the ratio between silicon (Si) and oxygen (O). Thus, the Raman scattering spectra described above, as well as the results of EDX measurements (see Table S1 in SM), allow us to state that there are no considerable changes in the crystallinity and chemical composition of SiNWs after the TA treatment.

Thermally induced evolution of the relative volume of voids

Firstly, we analyze the relative volume of voids (RVV) defined as the ratio between volume of empty space between nanowires and volume occupied by the whole SiNW array. The following experimental observation are taking into account: (i) reduction of the nanowires length after TA (as described above) and (ii) TA induced evolution of the SiNW morphology (see Fig. 1). The RVV value is estimated by means of the digital analysis of planar-view SEM images by using ImageJ software. Fig. 3 shows the dependence of RVV of as-prepared and TA treated SiNW arrays on MACE time, i.e. on the length of SiNWs. As can be seen, a huge decrease in the RVV values (> 2 times) is observed for the TA treated SiNWs in comparison with that for as-prepared ones. The most impressive structural difference is observed for the longest (26.3 μm) SiNWs: the corresponding RVV value decreases from 78% for as-prepared SiNWs to 29% for the TA treated samples.

Size distribution of voids

Typical size distributions of voids in as-prepared and TA treated SiNWs with initial length of 26.3 μm are shown in Fig. 4 and the corresponding results for the samples with other lengths are given in SM as Figs. S2 and S3. The obtaned data reveal an effect of the TA induced evolution of void sizes. Indeed, the majority of voids in as-prepared samples has dimension ranging from 20 to 60 nm. The following structural changes are observed in the TA treated SiNWs: (i) the surface density of voids (ratio of their number over the occupied area in μm^2) is significantly increased by almost one order of magnitude, (ii) the smallest sizes of voids shifted down to 10–20 nm, (iii) large voids with sizes > 110 nm appeared. The appearance of the large voids can be explained by the thermally activated aggregation of the smallest ones. As for the voids with dimensions less than 40 nm, the huge increase in

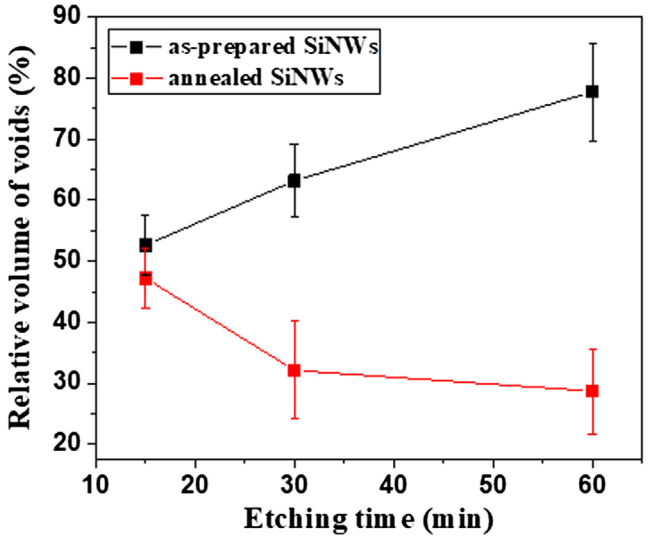

Fig. 3. Relative volume of voids versus etching time for SiNWs arrays before (black squares) and after (red squares) TA treatment.

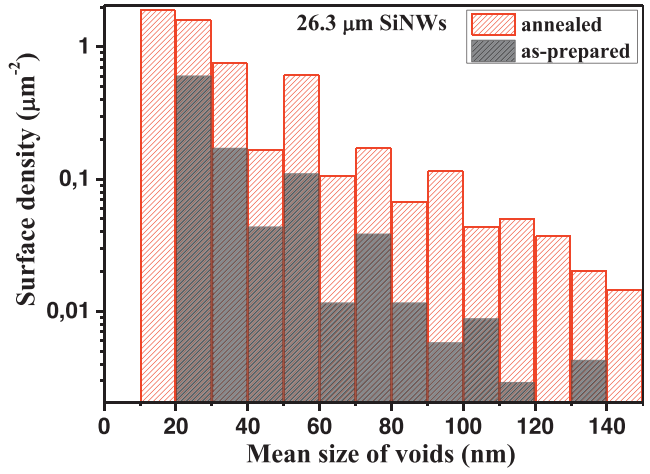

Fig. 4. Typical size distributions of voids in as-prepared and TA treated SiNWs with initial length of 26.3 μm.

their number is caused by thermally induced cracking of SiNWs complexes.

Theoretical analysis of thermally induced structural evolution

The above described TA induced evolution of the morphology of the SiNWs arrays is a typical manifestation of the well-known Ostwald ripening phenomenon [41,42] which can be quantitatively described by the Lifshitz-Slyozov-Wagner (LSW) theory [26–28]. We suppose that SiNW arrays posess a hollow crystalline structure supersaturated with vacancies. In general, the LSW theory distinguishes two stages of the formation of grains of a new phase due to diffusion effects in a supersaturated solid solution. In the first, concentration fluctuations produce nuclei of new phase, which grow directly from the supersaturated medium. The second stage may be considered to begin when the formed grains thus they have reached an appreciable size and the degree of supersaturation of the matrix has become very slight. In such circumstances, the growth of large grains of the new phase by the incorporation of small ones [26]. This is one of the well-established theories describing how vacancies evolve during annealing to achieve a final equilibrium state. The concept of the critical radius (r_c) is introduced in the LSW theory. If the variable radius of the void (r) is larger than r_c, the volume of voids increases. On the contrary, if $r < r_c$ the number of voids increases and their distribution over the radius (r) decreases. This mechanism explains how large voids "devour" small ones. Based on the LSW theory, it is possible to estimate the value of rc characterizing thermally induced evolution of voids in SiNW arrays.

According to the LSW theory the avarage radius of growing voids can be described by the following expression [26]:

$$\langle r\rangle^3 - \langle r\rangle_c^3 = \frac{8\gamma c_\infty v^2 D}{9R_g T}t \quad (1)$$

where $\langle r\rangle$ is the average radius of all the voids, γ is the surface energy, c_∞ is the solubility, v is the molar volume, D is the diffusion coefficient of the vacancies in c-Si, R_g is the ideal gas constant, T is the temperature and t is the TA treatment time.

In our case, at the fixed temperature and TA duration, Eq. (1) together with the theory parameters from Ref. [43,44] allow us to estimate $r_c \approx 60$ nm, i.e. the critical diameter of the void is about 120 nm, that is in agreement with size distribution of the voids shown in Fig. 4. as well as with the features related to the Oswald ripening phenomenon described above.

All the structural features of SiNWs arrays before and after annealing are schematically summarized in Fig. 5. In particular, the thermal annealing induces the dramatic decrease of SiNW length accompanied with a significant change in the number of small (10–40 nm) and large (> 110 nm) as well as a huge decrease of the RVV value described above.

Optical properties

Fig. 6 shows the total reflection spectra of as-prepared and TA treated SiNWs. As can be seen, the total reflection of as-prepared SiNWs (solid lines in Fig. 6) strongly depends on the nanowires length. In

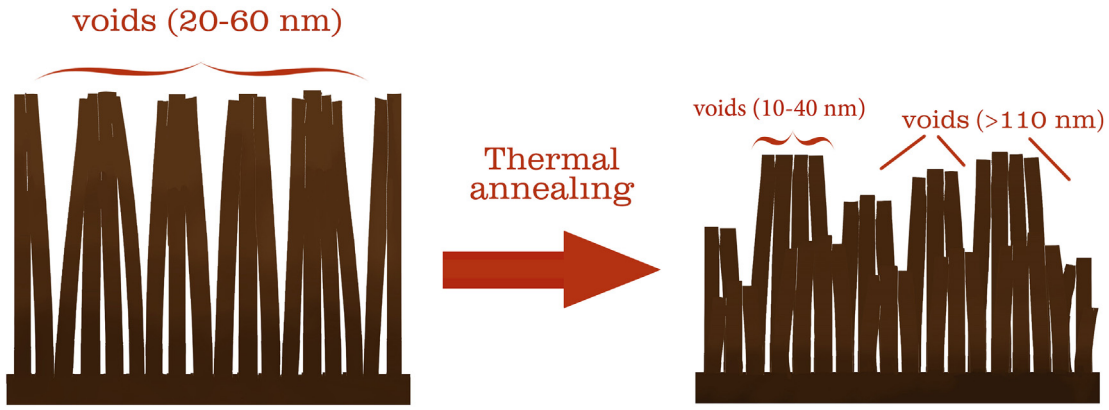

Fig. 5. Schematic view of structural changes in SiNWs array after TA treatment.

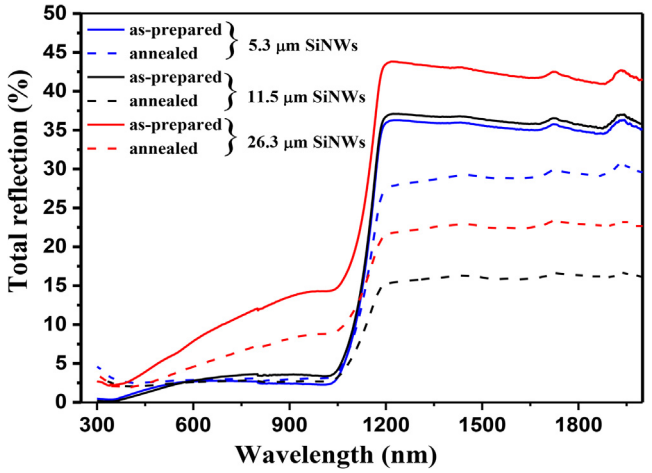

Fig. 6. Total reflection spectra of as-prepared and thermally annealed SiNW arrays with different initial lengths of SiNWs.

particular, the reflectivity increases with the length of nanowires. SiNWs arrays with lengths of 5.3 μm and 11.5 μm show the reflectance below 5% in the UV–VIS spectral region, which can be explained by partial localization of light due to its strong elastic scattering accompanied by absorption in Si nanocrystals [45]. For the 26.3 μm long SiNWs, we observe: (i) an increase in reflectance in the range of 500–1200 nm due to Mie scattering in Si nanostructures with dimensions comparable to light wavelength [46] and (ii) a high total reflectance in the spectral region above 1100 nm due to light scattering [17].

The total reflection spectra of the annealed SiNWs arrays (dashed lines in Fig. 6) demonstrates a significant decrease of the reflectance level in the whole (UV–VIS-IR) spectral range. Moreover, the thermally induced changes in the morphology of SiNWs lead to a 2-fold reduction in the total reflection coefficient in the IR region for nanowires longer than 11.3 μm.

Conclusions

The structural evolution occurring in crystalline SiNWs during the high temperature annealing was carefully investigated. The SEM data show that the thermal annealing of SiNWs at 900 °C results in the following structural modifications: (i) shortening of the mean length of SiNWs, (ii) decrease in the relative volume of voids, and (iii) significant changes in the pore size distribution.

These structural changes are explained by the Oswald ripening in SiNW arrays. The observed modification of SiNWs morphology correlates with significant changes in the optical properties of SiNW arrays measured in the range from 300 nm to 2000 nm. The obtained results can be useful for tailoring the structure and optical properties of SiNWs for various applications.

CRediT authorship contribution statement

Gauhar Mussabek: Conceptualization, Methodology, Writing - original draft, Writing - review & editing, Funding acquisition. **Vladimir Lysenko:** Conceptualization, Writing - review & editing. **Dana Yermukhamed:** Validation, Investigation, Data curation, Writing - review & editing. **Vladimir Sivakov:** Methodology, Project administration, Writing - review & editing. **Victor Yu. Timoshenko:** Supervision, Writing - review & editing.

Declaration of Competing Interest

The authors declare that they have no known competing financial interests or personal relationships that could have appeared to influence the work reported in this paper.

Acknowledgments

The work was partially supported by the Committee of Science of the Ministry of Education and Science of the Republic of Kazakhstan (Grant No.AP05133366). G. M. and V.S. are grateful to the German Academic Exchange Service (DAAD) for individual Scholarship in frame of the Research Stays for University Academics and Scientists (2018) funding programme at Leibniz Institute of Photonic Technology in Jena/Germany. V.Yu.T. thanks the support from the MEPhI Academic Excellence Project (Agreement with the Ministry of Education and Science of the Russian Federation of 27.08.2013, project #02.a03.21.0005).

Data availability

The raw data required to reproduce these findings cannot be shared at this time due to technical or time limitations. The processed data required to reproduce these findings cannot be shared at this time due to technical or time limitations.

Appendix A. Supplementary data

Supplementary data to this article can be found online at https://doi.org/10.1016/j.rinp.2020.103258.

References

[1] Saxena A, Kumar M, Sharma RK, Gupta RS. SOI Schottky barrier nanowire MOSFET with reduced ambipolarity and enhanced electrostatic integrity. J Electron Mater 2020;49:4450–6. https://doi.org/10.1007/s11664-020-08164-0.
[2] Sessi V, Simon M, Mulaosmanovic H, Pohl D, Loeffler M, Mauersberg T, et al. A silicon nanowire ferroelectric field-effect transistor. Adv Electron Mater 2020;6(4):1901244. https://doi.org/10.1002/aelm.201901244.
[3] Kolay A, Maity D, Ghosal P, Deepa M. Carbon@Tellurium nanostructures anchored to a Si nanowire scaffold with an unprecedented liquid-junction solar cell performance. ACS Appl Mater Interfaces 2019;11(51):47972–83. https://doi.org/10.1021/acsami.9b17573.
[4] Yu P, Wu J, Liu Sh, Xiong J, Jagadish C, Wang ZM. Design and fabrication of silicon nanowires towards efficient solar cells. Nano Today 2016;11(6):704–37. https://doi.org/10.1016/j.nantod.2016.10.001.
[5] Gudovskikh AS, Morozov IA, Kudryashov DA, Nikitina EV, Sivakov V. Multijunction a-Si:H/c-Si solar cells with vertically-aligned architecture based on silicon nanowires. Mater Today: Proc 2017;4(7):6797–803. https://doi.org/10.1016/j.matpr.2017.07.006.
[6] Bauer D, Luisier M. Influence of disorder and surface roughness on the electrical and thermal properties of lithiated silicon nanowires. J Appl Phys 2020;127:135101https://doi.org/10.1063/5.0002980.
[7] Diez GG, Gordillo JMS, Pujado MP, Salleras M, Fonseca L, Morata A, et al. Enhanced thermoelectric figure of merit of individual Si nanowires with ultralow contact resistances. Nano Energy 2020;67:104191https://doi.org/10.1016/j.nanoen.2019.104191.
[8] Timoshenko VY. Silicon nanocrystals: physical properties and potential biomedical applications. Phys Sci Technol 2017;4:59–73https://doi.org/10.26577/phst-2017-2-135.
[9] Saha P, Dash DK, Sarkar SK. Nanowire reconfigurable FET as biosensor: Based on dielectric modulation approach. Solid State Electron 2019;161:107637https://doi.org/10.1016/j.sse.2019.107637.
[10] Piedimonte P, Mazzetta I, Fucile S, Limatola C, Cattaruzza E, Riello P, et al. Silicon nanowires to detect electric signals from living cells. Mater Res Express 2019;6(8):084005https://doi.org/10.1088/2053-1591/ab20f8.
[11] Manjunatha KN, Paul S. In-situ catalyst mediated growth and self-doped silicon nanowires for use in nanowire solar cells. Vacuum 2017;139:178–84. https://doi.org/10.1016/j.vacuum.2016.12.002.
[12] Solanki A, Um H. Chapter two – top-down etching of Si nanowires. Semiconduct Semimetals 2018;98:71–149. https://doi.org/10.1016/bs.semsem.2018.04.001.
[13] Sandu G, Osses JA, Luciano M, Caina D, Stopin A, Bonifazi D, et al. Kinked silicon nanowires: superstructures by metal-assisted chemical etching. Nano Lett 2019;19(11):7681–90. https://doi.org/10.1021/acs.nanolett.9b02568.
[14] Perez-Diaz O, Quiroga-Gonzalez E. Silicon conical structures by metal assisted chemical etching. Micromachines 2020;11(4):402. https://doi.org/10.3390/mi11040402.
[15] Wendisch FJ, Abazari M, Mahdavi H, Rey M, Vogel N, Musso M, et al. Morphology-graded silicon nanowire arrays via chemical etching: engineering optical properties

at the nanoscale and macroscale. ACS Appl Mater Interfaces 2020;12(11):13140–7. https://doi.org/10.1021/acsami.9b21466.
[16] Lv J, Zhang T, Zhang P, Zhao Y, Li Sh. Review application of nanostructured black silicon. Nanoscale Res Lett 2018;13:110. https://doi.org/10.1186/s11671-018-2523-4.
[17] Mussabek GK, Yermukhamed D, Suleimenova ZA, Assilbayeva RB, Sivakov VA, Zavestovskaya IN, et al. Reflectance modification in nanostructured silicon layers with gradient porosity. Bull. Lebedev Phys. Inst. 2019;46:314–8. https://doi.org/10.3103/S106833561910004X.
[18] Wippermann S, He Yu, Voros M, Galli G. Novel silicon phases and nanostructures for solar energy conversion. Appl Phys Rev 2016;3:040807https://doi.org/10.1063/1.4961724.
[19] Savin H, Repo P, von Gastrow G, Ortega P, Calle E, Garín M, et al. Black silicon solar cells with interdigitated back-contacts achieve 22.1% efficiency. Nat Nanotechnol 2015;10:624–8. https://doi.org/10.1038/nnano.2015.89.
[20] Moghimi MJ, Lin G, Jiang H. Broadband and ultrathin infrared stealth sheets. Adv Eng Mater 2018;20:1800038. https://doi.org/10.1002/adem.201800038.
[21] Fazio B, Artoni P, Iatì MA, et al. Strongly enhanced light trapping in a two-dimensional silicon nanowire random fractal array. Light Sci Appl 2016;5:e16062https://doi.org/10.1038/lsa.2016.62.
[22] Rashid M, Ahmed NM, Noor NAMd, Pakhuruddin MZ. Silicon quantum dot/black silicon hybrid nanostructure for broadband reflection reduction. Mater Sci Semicond Process 2020;115:105113https://doi.org/10.1016/j.mssp.2020.105113.
[23] Shoo MK, Kale P. Integration of silicon nanowires in solar cell structure for efficiency enhancement: a review. J Materiomics 2019;5:34–48. https://doi.org/10.1016/j.jmat.2018.11.007.
[24] Qin Yu, Wang Z, Liu D, Wang K. Dendritic composite array of silicon nanowires/WO_3 nanowires for sensitive detection of NO_2 at room temperature. Mater Lett 2017;207:29–32. https://doi.org/10.1016/j.matlet.2017.07.042.
[25] Pinnelli G. Top-down fabrication of silicon nanowire devices for thermoelectric applications: properties and perspectives. Eur Phys J B 2015;88:121. https://doi.org/10.1140/epjb/e2015-50638-0.
[26] Lifshitz IM, Slyozov VV. The kinetics of precipitation from supersaturated solid solutions. J Phys Chem Solids 1961;19:35–50. https://doi.org/10.1016/0022-3697(61)90054-3.
[27] Wagner C. Z. Theorie der alterung von niederschlagen durch umlosen (Ostwald-Reifung). Elektrochem 1961;65:581–91.
[28] Geguzin JE. The physics of sintering. 2nd ed. M: Nauka; 1984. p. 312. (in Russian).
[29] Elia P, Nativ-Roth E, Zeiri Y, Porat Z. Determination of the average pore-size and total porosity in porous silicon layers by image processing of SEM micrographs. Mesopor Mat 2016;225:465–71. https://doi.org/10.1016/j.micromeso.2016.01.007.
[30] Lipkova EA, Efimova AI, Gonchar KA, Presnov DE, Eliseev AA, Lapin AN, et al. Determination of the free charge carrier concentration in boron-doped silicon nanowires using attenuated total reflection infrared spectroscopy. Semiconductors 2019;53:1524–8. https://doi.org/10.1134/S1063782619110113.
[31] Ogata YH, Yoshimi N, Yasuda R, Tsuboi T, Sakka T, Otsuki A. Structural change in p-type porous silicon by thermal annealing. J Appl Phys 2001;90:6487–92. https://doi.org/10.1063/1.1416862.
[32] Lide DR. Handbook of Chemistry and Physics. 82nd ed. London: CRC; 2001–2002.
[33] Sivakov V, Scholz R, Syrowatka F, Falk F, Gosele U, Christiansen SH. Silicon nanowire oxidation: the influence of sidewall structure and gold distribution. Nanotechnology 2009;20:405607https://doi.org/10.1088/0957-4484/20/40/405607.
[34] Ott N, Nerding M, Muller G, Brendel R, Strunk HP. Evolution of the microstructure during annealing of porous silicon multilayers. J Appl Phys 2004;95:497–503. https://doi.org/10.1063/1.1633657.
[35] Muller G, Nerding M, Ott N, Strunk HP, Brendel R. Sintering of porous silicon. Phys Status Solidi A 2003;197:83–7. https://doi.org/10.1002/pssa.200306472.
[36] Ott N, Nerding M, Muller G, Brendel R, Strunk HP. Structural changes in porous silicon during annealing. Phys Status Solidi A 2003;197:93–7. https://doi.org/10.1002/pssa.200306474.
[37] Fauchet PM. The Raman line shape of semiconductor nanocrystals. In: Lockwood DJ, Young JF, editors. Light scattering in semiconductor structures and superlattices. NATO ASI Series (Series B: Physics). Boston, MA: Springer; 1991.
[38] Iatsunskyi I, Nowaczyk G, Jurg S, Fedorenko V, Pavlenko M, Smyntyna V. One and two-phonon Raman scattering from nanostructured silicon. Optik 2015;126:1650–5. https://doi.org/10.1016/j.ijleo.2015.05.088.
[39] Yakunin VG, Asilbaeva RB, Rodichkina SP, Alykova AF, Turmukhambetov AZ, Timoshenko VYu. Raman spectroscopy of silicon nanowires formed by metal-assisted chemical etching. J Phys: Conf Ser 2019;1348:012025. https://doi.org/10.1088/1742-6596/1348/1/012025.
[40] Sivakov V, Voigt F, Berger A, Bauer G, Christiansen SH. Roughness of silicon nanowire sidewalls and room temperature photoluminescence. Phys Rev B. 2010;82:125446https://doi.org/10.1103/PhysRevB.82.125446.
[41] Zeng HC. Ostwald ripening: a synthetic approach for hollow nanomaterials. Curr Nanosci 2007;3:177–81. https://doi.org/10.2174/157341307780619279.
[42] Tutashkonko S, Nychyporuk T, Lysenko V, Lemiti M. Thermally induced Oswald ripening of mesoporous Ge nanostructures. J Appl Phys 2013;113:023517https://doi.org/10.1063/1.4775576.
[43] Vanhellemont J, Simoen E. Brother silicon, sister germanium. J. Electrochem 2007;154(7):H572–83. https://doi.org/10.1149/1.2732221.
[44] Eustathopoulos N, Drevet B. Surface tension of liquid silicon: High or low value? J Cryst Growth 2013;372:77–83. https://doi.org/10.1016/j.jcrysgro.2013.02.010.
[45] Osminkina LA, Gonchar KA, Marshov VS, Bunkov KV, Petrov DV, Golovan LA, et al. Optical properties of silicon nanowire arrays formed by metal-assisted chemical etching: evidences for light localization effect. Nanosc Res Lett 2012;7:524. https://doi.org/10.1186/1556-276X-7-524.
[46] Brönstrup G, Garwe F, Csaki A, Fritzsche W, Steinbruck A, Christiansen S. Statistical model on the optical properties of silicon nanowire mats. Phys. Rev. B 2011;84:125432https://doi.org/10.1103/PhysRevB.84.125432.